

CFD-BASED DESIGN OPTIMIZATION FOR A SINGLE ELEMENT ROCKET INJECTOR

Rajkumar Vaidyanathan^{(1)*}, P. Kevin Tucker^{(2)†}, Nilay Papila^{(1) †} and Wei Shyy^{(1)‡}

⁽¹⁾Department of Mechanical and Aerospace Engineering

University of Florida, Gainesville, FL 32611.

⁽²⁾NASA Marshall Space Flight Center

MS/TD64, MSFC, AL 35812

ABSTRACT

A CFD-based design optimization approach has been proposed for a single element rocket injector. The overall goal of the effort is to demonstrate the integration of a set of tools that allows the injector designer to objectively determine the trades between performance and life. Using design of experiment techniques, 54 cases are selected and computational solutions based on the Navier-Stokes equations, finite rate chemistry, and the $k-\epsilon$ turbulence closure are obtained. The response surface methodology is employed as the optimization tool. Design evaluations are guided by four design objectives. The maximum temperature on the injector element oxidizer post tip, the maximum temperature on the injector face and a combustion chamber wall temperature are chosen as life indicators. The length of the combustion zone is selected as an indicator of mixing and performance. Four independent design variables are selected, namely, H_2 flow angle, H_2 and O_2 flow areas with fixed flow rates, and O_2 post tip thickness. In the context of this effort, the design optimization tools performed efficiently and reliably. In addition to establishing optimum designs by varying emphasis on the individual objectives, better insight into the interplay between design variables and their impact on the design objectives is gained. The need to include environmental design objectives early in the design phase is clearly established.

1. INTRODUCTION

The Space Shuttle has been propelled into space for the last 20 years by the world's most sophisticated reusable engine, the Space Shuttle Main Engine (SSME). In spite of its impressive performance, the SSME lacks robustness, especially in the combustion devices and turbomachinery areas, creating significant reliability issues. The resulting frequency and level of maintenance create very high operational costs. The goal of NASA's Next Generation Launch Technology (NGLT) Program is to develop technologies to make the next generation launch systems safer, more affordable and more reliable.

* Graduate Student Assistant, Student Member AIAA

† Aerospace Engineer, Member AIAA

‡ Professor and Department Chair, Fellow AIAA

Copyright ♥ 2003 by authors. Published by the American Institute of Aeronautics and Astronautics, Inc., with Permission.

The design of robust, long-life combustion devices, namely, injectors, chambers and nozzles, will be an important element in meeting these ambitious goals. From a component life standpoint, the injector design is a key factor. Both performance and thrust chamber environments are governed in large part by the injector design. The thrust chamber performance is determined by the rate and the extent to which mixing and resultant combustion occurs. This mixing efficiency and performance are functions of the details of the injector design. On the other hand, the location of the mixing and resultant combustion is the key factor in determining the injector and thrust chamber thermal environments. These environments, which relate directly to component life, include temperatures on the combustor wall, injector face and for coaxial injectors, the oxidizer post tip. The difficulty encountered in designing injectors that perform well and have manageable environments is that the factors that promote performance often lead to increased heating of the solid surfaces on the injector and combustor.

Current injector design tools have been in use for 30 years or more¹⁻⁵ and are largely empirical-based. The experimental databases, and thus the tools developed from them, are limited, in terms of design space, to specific element configurations that have been tested⁶. In terms of scope, the design tools typically focus on performance, with the environment being a secondary consideration. The limited amount of environmental information available from these tools is usually one-dimensional and not functionally related to details of the injector design. It is very doubtful that application of these traditional design tools will result in future propulsion devices that successfully address the NGLT goals noted above.

The advent and advancement of computational fluid dynamics (CFD) in the last 20 years has produced a capability that has shown potential as an improved design tool in many areas of rocket propulsion. However, there are three requirements that the CFD tool must meet before it can be routinely employed in the rocket component design process. First, CFD solutions must provide an increased fidelity level relative to the historical tools in terms of geometry representation and physical modeling. Second, a rigorous validation process is required before the designer can confidently employ CFD as a tool for quantitative decision-making. Finally,

generation of significant quantities of parametric solutions must be possible during the design cycle time frame.

The application of CFD to injector design has lagged behind other areas such as turbomachinery because the physical models are more complicated for multiphase, turbulent reacting flows. Unfortunately, the same features that make CFD a promising injector design tool have also retarded its use for injector design. Progress in meeting the three requirements noted above has been uneven. For example, new models that efficiently account for some of the complex processes⁷ and thus increase the solution fidelity have recently become available. However, the three-dimensional geometry of multi-element injectors and the complex physical processes inherent in the flows that issue from them create major obstacles in the other two areas in terms of using CFD as a design tool. The harsh high pressure and temperature environments typical of injector flows create significant difficulty in obtaining experimental data of satisfactory quality to validate and guide further development of computational models. Finally, solving the equations, for multiphase reacting flows, with high resolution typically requires lengthy computational times. However, continuing increases in computer speed and progress in parallel processing have begun to mitigate this turnaround problem.

It has long been known that small changes in injector geometry can have significant impact on performance⁸, as well as on environmental variables such as combustion chamber wall and injector face temperatures and heat fluxes. CFD can be used to account for several independent geometric variables over appropriate ranges by calculating the performance and environmental variables, which impact NGLT design goals. To effectively accomplish this multi-objective exercise, an optimization technique is desirable to assist and guide the designer in objective management of the complex and competing trends embodied in the CFD-generated data.

2. SCOPE & APPROACH

In the present effort, a CFD-based design/optimization methodology for single element injectors is proposed and applied to an injector that is a representative of the elements being considered for certain NGLT engine cycles. While the ultimate goal is to analyze multi-element injectors, much of the detailed work in injector design can be done, or at least initiated, at the single element level. In the present effort, the focus is on a design methodology for a single element injector. CFD solutions based on the Navier-Stokes equations, finite rate chemistry and the k - ϵ turbulence closure are obtained on injector designs generated by design of experiment (DOE) techniques^{9,10}. The response surface methodology (RSM)⁹ is employed as the optimization

tool. As a proof of the concept, the CFD-based optimization strategy is demonstrated in the context of a coaxial element using gaseous oxygen (GO_2) and gaseous hydrogen (GH_2) propellants represented in Figure 1. Four independent design variables are selected, namely, H_2 flow angle, H_2 and O_2 flow areas with fixed mass flow rates of fuel and oxidizer and Q post tip thickness. The design evaluation is guided by four design objectives. Objectives that are life indicators include the maximum temperature on the oxidizer post tip, the maximum temperature on the injector face and a combustion chamber wall temperature taken three inches from the injector face. The performance indicator considered is the length of the combustion zone. Taken together, they provide a basic framework to facilitate exploration of the issues. Additional details for all the independent and dependent variables are provided in the section describing the injector model.

To facilitate the development of the present methodology, a baseline element design is needed as a starting point. This baseline concept is generated by an empirical design methodology based on a specific set of propellant flow rates, mixture ratio and chamber pressure. The selected design variables are then varied based on this baseline design and the design space populated with the aid of a DOE technique. The prescribed CFD cases are executed and post processed to extract the required dependent variable data. This data is then used to generate a response surface for each dependent variable in terms of the independent variables, and an optimization technique is applied to identify suitable designs. Details on these concepts and processes will be provided after describing the injector model.

The response surface generation is evaluated for two grids of different resolutions and the relationship between the optimization process and CFD solution process is explored. Finally, the response surfaces are used in three separate optimization examples demonstrating the utility and flexibility of the methodology.

2.1 Injector Model

Liquid rocket propulsion injector elements can be categorized into two basic types based on propellant mixing. The first type is an impinging element (Figure 2a) where mixing occurs by direct impingement of the propellant streams at an acute angle. The impingement enhances mixing by head-on interaction between the oxidizer and fuel⁸. The second type of injector consists of non-impinging elements where the propellant streams flow in parallel, typically in coaxial fashion (Figure 2b). Here, mixing is accomplished through a shear-mixing processes¹¹.

From a design standpoint, both element types have appealing characteristics. However both also have undesirable characteristics. For instance, if the impinging element has an F-O-F arrangement (Figure 2a), the

mixing occurs rapidly, which can yield high performance. However, since the combustion zone is close to the injector face, the potential for high levels of injector face heating must be considered. If the non-impinging element is assumed to be a shear coaxial element, mixing across the shear layer is relatively slow⁸, requiring longer chambers to allow complete combustion. However, since the combustion zone is spread over a longer axial distance, the injector face is generally exposed to less severe thermal environments.

Important design parameters for the impinging element (assuming fixed mass flow rates and constant propellant inlet conditions) include relative orifice size (or, relative stream momentum ratio), impingement angle and orifice spacing. Important parameters for the shear coaxial element (assuming fixed mass flow rates and constant propellant inlet conditions) include the area ratio of the two concentric tubes (or velocity ratio) and the shear area between the two propellant streams (i.e., the oxidizer post tip thickness)¹¹.

Of course, one can combine the above-mentioned characteristics of injector types to develop hybrid concepts. For example, it has been noted⁸ that performance improvement in the shear coaxial element can be realized by directing the fuel toward the oxidizer stream rather than parallel to it and thinning the oxidizer post wall. The first modification causes the shear coaxial element to take on some of the aspects of the F-O-F impinging element. These notions lead to the hybrid element shown in Figure 1 that has been developed by The Boeing Company (U. S. Patent 6253539).

The four independent design variables chosen for the element, used in this study, are shown in Figure 3a. They are the angle at which the H₂ is directed toward the oxidizer, Variable-1 (α), the change in H₂ flow area from a baseline area, Variable-2 (ΔHA), the change in O₂ flow area from a baseline area, Variable-3 (ΔOA), and the oxidizer post tip thickness, Variable-4 (OPTT). The fuel and oxidizer flow rates are held constant. The independent variable ranges considered in this exercise are shown in Table 1.

The dependent variables chosen for design evaluation are shown in Figure 3b. They are the maximum injector face temperature, Objective-1 (TF_{max}), the wall temperature at a distance three inches from the injector face, Objective-2 (TW₄), the maximum oxidizer post tip temperature, Objective-3 (TT_{max}) and centerline axial location where the combustion is 99% complete, Objective-4 (hereafter referred to as the combustion length, X_{cc}) (Figure 3b). The three temperatures (calculated as adiabatic wall temperatures in this study) were chosen as indicators of local environments. Lower temperatures would indicate a design that had longer life due to decreased thermal strain on the part. The combustion length, Objective-4 (X_{cc}), was chosen as a measure of performance. Shorter combustion lengths indicate better performing designs.

Comparison of two of the evaluated designs serves to illustrate the motivation for combining CFD analyses and an efficient optimization technique in the design process. The independent design variables, normalized between 0 and 1, are shown for the two cases in Table 2. In terms of the design space evaluated, these two designs are seen to be quite different. The normalized dependent variables are also shown in Table 2 with the temperatures shown in contour plots (Figures 4 and 5).

The chamber wall and injector face temperatures for Case Y (as seen in Figure 4) are low or moderately low, while for Case X, they are high. Figure 6 shows a large recirculation zone located between the injector and the chamber wall. This recirculating flow strips hot gases from the flame and causes them to flow back along the chamber wall and injector face. This phenomenon regulates the chamber wall temperature (Objective-2 (TW₄)) and the injector face temperature (Objective-1 (TF_{max})). Figure 5 shows that the other life-indicating variable, the maximum oxidizer post tip temperature (Objective 3 (TT_{max})) has essentially the opposite trend as compared to the other two temperatures.

The performance indicator, combustion length (Objective-4 (X_{cc})) is seen (Table 2) to be at a minimum level for Case X (shorter combustion lengths indicate better mixing elements) and at a moderate level for Case Y. Given these observations, it is clear that the dependent variables exhibit competing trends such that no design will produce the "best" values for all the dependent variables.

These comparisons confirm the earlier statement that changes in the injector design details have major effects on injector performance and injector-generated environments. These, and ultimately, other relevant geometric details, must then be accounted for by the new design tool. Injector designs addressing NGLT goals must be produced by a tool that not only predicts performance, but accounts for multiple, spatially resolved environmental variables. Efficient, validated CFD codes that model sufficient injector physics are necessary to meet these requirements.

Generation of large amounts of complex information by these codes produces the need for a means to manage the data. The injector designer must be able to confidently and efficiently sort through this database to locate an acceptable compromise design. A global optimization technique is an ideal tool to address this goal. It uses the information to generate a map of the complete design space, which can then be used to guide the designer to useful designs. This effort will demonstrate that RSM is a global optimization technique that meets this requirement.

2.2 Numerical Procedure

A pressure-based, finite difference, Navier-Stokes solver, FDNS500-CVS¹²⁻¹⁴, is used in this study. The Navier-Stokes equations, the two-equation turbulence

model, and kinetic equations are solved. Convection terms are discretized using either a second order upwind, third order upwind or a central difference scheme, with adaptively added second order and fourth order dissipation terms. For the viscous and source terms, second order central differencing scheme is used. First order upwind scheme is used for scalar quantities, like turbulence kinetic energy and species mass fractions, to ensure positive values. Steady state is assumed and an implicit Euler time marching scheme is used for computational efficiency. The chemical species continuity equations represent the H₂ - O₂ chemistry. It is represented with the aid of a 7-species and 9-reaction set¹²⁻¹⁴. The simulation domain and the boundary conditions used in all the CFD cases are shown in Figure 7. Because of the very large aspect ratio, both the injector and chamber have been shortened (at the cross hatched areas) for clarity. Both fuel and oxidizer flow in through the west boundary where the mass flow rate is fixed for both streams. The nozzle exit, at the east boundary, is modeled by an outlet boundary condition. The south boundary is modeled with the symmetry condition. All walls (both sides of the oxygen post, the outside of the fuel annulus, the outside chamber wall, and the faceplate) are modeled with the no slip adiabatic wall boundary condition.

2.3 Design of Experiments

The predictive capability of a response surface (RS) is largely dependent on the selection of the design space as it dictates the distribution of the available information. There are different types of design of experiments techniques. Among various alternatives, the orthogonal array (OA)¹⁵, which is an efficient approach, is used here. An OA is a fractional factorial matrix that assures a balanced comparison of levels of any factor or interaction of factors¹⁵. A matrix A with elements a_i^j is called an OA. In this notation j shows the row ($j = 1, 2, \dots, n_r$) and i shows the column ($i = 1, 2, \dots, n_c$) that a_i^j belongs to, supposing that each $a_i^j \in Q = \{0, 1, \dots, q-1\}$. This matrix is of strength $t \leq n_c$ if in each n_r -row-by- t -column sub-matrix of all q^t possible distinct rows occur λ times. Such an array is denoted by $OA(n_r, n_c, q, t)$ by Owen¹⁵. Based on the DOE theory, orthogonal arrays can significantly reduce the number of experimental configurations. Information directly relevant to the use of OA can be found in the works of Shyy et al.¹⁶ and Papila¹⁷.

In the present study, using the OA technique, 54 designs are generated for fitting and testing the response surface. To test the RS, 14 of the 54 designs are selected using cross-validation techniques. Cross-validation¹⁷ is an established technique for estimating the prediction accuracy. This method is usually performed using either a number of random test/train partitions of the data, or k -fold cross-validation¹⁸. During the CFD computations,

two of the 40 designs (training set) were found to be unacceptable because they exhibited unsteady behaviors while the numerical algorithm was based on the steady state model. Hence, the final information included 38 designs for training the RS and 14 to test their predictive capabilities. All the design variables are normalized between 0 and 1 based on their maximum and minimum values. All the responses obtained from the CFD solutions of the 52 valid designs are scaled to O(1) and RS generated. Once the RS are generated, the responses are renormalized between 0 and 1 based on the maximum and minimum of the generated RS, which will be referred to as the normalized responses in the text. These normalized values are used in this paper. The training and testing designs are shown in Table A1 in the appendix. It should be noted that when the Variable-3 (ΔOA) is 1 or 0, the O₂ flow area is reduced by 0% or 40%, respectively, as compared to the baseline area.

2.4 Response Surface Methodology

The response surface methodology is adopted in the present study. This technique is effective in representing the global characteristics of the design space and it filters noise associated with design data. However, depending on the order of polynomial employed and the shape of the actual response surface, the RSM can introduce substantial errors due to its generally low order representation. Additionally, the number of design points needed to construct a response surface increase rapidly with the number of design variables. For example, for a second order response surface, the number of coefficients associated with the polynomial scales with the number of design variables, N , as $(N+1)(N+2)/(2!)$, while a third order polynomial scales as $(N+1)(N+2)(N+3)/(3!)$.

In this study, the response surfaces are fit with n^{th} order polynomials using standard least-squares regression. Statistical analysis software, JMP¹⁹, is used for the generation of the polynomials. In the standard least-squares regression method, based on t-statistics⁹, terms with least influence in the prediction are discarded and the prediction improved, which gives the reduced model. The quality of fit between different surfaces can be evaluated by comparing the adjusted RMS error⁹, σ_a , defined as:

$$\sigma_a = \sqrt{\frac{\sum \epsilon_i^2}{n-p}} \quad (1)$$

where ϵ_i is the error at the i^{th} point, n is the number of data points and p is the number of coefficients. The measure of error given by σ_a is normalized to account for the degrees of freedom in the model. This adjusted RMS error thus accounts for the nominal effect of higher order terms providing a better overall comparison among the different surface fits. Another measure of error, the

adjusted coefficient of multiple determination⁹, R_a^2 , measures the proportion of variation in the response around the mean that can be attributed to terms in the model rather than to random error. It is given by

$$R_a^2 = 1 - \frac{\sigma_a^2}{SS_{yy}/(n-1)} \quad (2)$$

where SS_{yy} is the sum of squares of error about the mean of the observations. For a good fit, R_a^2 should be closer to one. The RMS error, σ , for the test data is given by:

$$\sigma = \sqrt{\frac{\sum e_i^2}{m}} \quad (3)$$

In this equation, e_i is the error at the i^{th} test point and m is the number of test points. For a good model the difference between σ_a and σ should not be large.

In certain cases, especially when higher order polynomials are used, the number of CFD computations may not be adequate to spare enough data for testing the RS. Hence, an alternate method to estimate the performance of the RS is to compute the PRESS statistic. The method proposed by Allen^{20, 21} computes a residual sum of squares. This residual is obtained by fitting a RS over the design space after dropping one design point from the training set and then comparing the RS predicted value for that point with the expected value. The PRESS RMS error is given by

$$PRESS_{ms} = \sqrt{\frac{\sum_{i=1}^n [y_i - \hat{y}_i]^2}{n}} \quad (4)$$

where y_i is the expected value, \hat{y}_i is the value predicted by the RS for the i^{th} point, which is excluded while generating the RS and n is the number of design points. If this value is close to σ_a then the model performs well.

2.5 Construction of Multi-Objective Optimization

The optimization problem at hand can be formulated as

$$\begin{aligned} & \min \{f(\mathbf{x}), \mathbf{x} = (x_1, x_2, \dots, x_n)^T\} \\ & \text{subject to } lb \leq x_i \leq ub, \end{aligned}$$

where lb and ub are the lower and upper bound, respectively, of the design variable x . In the current study, different combinations of the objective functions are used to investigate the issues related to multi-objective optimization. One method of optimizing multiple responses simultaneously is to build, from the individual responses, a composite response known as the desirability function⁹. The method allows for a

designer's own priorities, concerning the response values, to be included in the optimization procedure. The first step in the method is to normalize the responses by developing a desirability function, d_i for each response, i . In the case where a response is to be minimized, the desirability takes on the form:

$$d_i = \left(\frac{F - A}{B - A} \right)^s, B \leq F \leq A \quad (5)$$

where F is the prediction of the RS, B is the target value and A is the highest acceptable value such that $d_i = 1$ for any $F \leq B$ and $d_i = 0$ for $F > A$. Hence, to minimize a response, this function has to be maximized. Choices for A and B are made according to the designer's priorities (e.g., maximum and minimum, respectively, of the individual RS in the present study). The sensitivity of the parameter, s , illustrated in Figure 8 can be instructive⁹. Desirability functions with $s \ll 1$ imply that a product need not be close to the response target value, B , to be quite acceptable. However, $s = 8$, implies that the product is nearly unacceptable unless the response is close to B .

The value of s is set based on which response has higher priority for the designer. A single composite response is developed which is the geometric mean of the desirability functions of the individual responses. The composite response is defined as:

$$D = (d_1 \cdot d_2 \cdot d_3 \cdots d_m)^{1/m} \quad (6)$$

where m is the number of objectives, which is then maximized. This approach was adopted in our previous efforts¹⁶ and has been found to be useful.

The optimization problem is then solved using *Solver*, an optimization tool available as part of *Microsoft Excel* package²². This tool uses the *Generalized Reduced Gradient (GRG2)* nonlinear optimization code developed by Lasdon et al.²³. The optimum solutions are then compared with CFD computations. Since the responses are scaled to O(1), the error measures have to be accordingly scaled to estimate the accuracy of the obtained solutions. In terms of the actual values the error for a response is defined as

$$\text{error} = \frac{|y_{CFD} - y_{RS}|}{y_{CFD}} \quad (7)$$

where y_{CFD} is the solution obtained from the CFD computation and y_{RS} is the prediction of the RS. Using simple mathematics, not shown here, the error in the scaled variables can be written as

$$error = \frac{|\bar{y}_{CFD} - \bar{y}_{RS}|}{\bar{y}_{CFD} + K} \quad (8)$$

where the bar represents the scaled values, and K is defined as

$$K = \frac{y_{min}}{y_{max} - y_{min}} \quad (9)$$

Here y_{min} and y_{max} are the actual minimum and maximum values, respectively, based on the available set of training and testing data for that response.

3. RESULTS AND DISCUSSION

3.1 Grid Sensitivity Investigation

Initially the 54 cases identified by DOE were computed on an axisymmetric geometry with 336·81 nodes. Only 33 out of the 40 training cases gave valid results. Results of the remaining seven cases contained unsteady features, which do not represent solutions of the steady state model employed. The RSs generated with these data for Objectives-3 and 4 (TT_{max} and X_{cc} , respectively) had R_a^2 values of 0.961 and 0.976, respectively, suggesting a less than desirable fit. On checking the grid distribution in the combustion zone for the 33 cases used, it was determined that the grid resolution was insufficient. After a series of tests involving addition of grid points in the axial direction in the combustion zone, a 430·81 grid was found to be appropriate and used for the second run of the optimization study. To highlight the grid refinement, a comparison of the grid distributions is shown in Figure 9. The final grid was the product of tripling the axial node density in the combustion zone. The thick red lines show the initial grid density, while the thin black lines show final grid density. Note that, for clarity, only every sixth j-line is shown. New RSs were generated from new solutions obtained on the fine grid. The new fits for Objectives-3 and 4 (TT_{max} and X_{cc} , respectively) had R_a^2 values of 0.989 and 0.995, respectively, representing a considerable improvement over the RS performance based on the first, coarser grid. This time, only two out of the 40 designs failed to produce valid results. It is to be noted that the R_a^2 values for Objectives-1 and 2 (TF_{max} and TW_4 , respectively) are 0.999 for both the initial and final grid. This experience indicates that in addition to facilitating design optimization, the RSM can also help address the adequacy of the CFD solution accuracy. It offers insight into potential problems, based on the statistical regressions, from which the computations can be refined, thus improving the fidelity of the individual and collective databases. While this approach does not guarantee universally satisfactory outcomes, it does suggest clear directions to assess the critical area of data quality.

3.2 Optimization Process

In the following, data for each dependent variable from the 38 acceptable training cases were used to generate the RS. Both full and reduced quadratic polynomials are generated. Table 3 identifies σ_a and σ for the four objective functions and different polynomials generated. The full quadratic model is consistent in performance in terms of both σ_a and σ . The reduced quadratic models either have a poorer value of σ or offer only marginal improvement over the full response surface model. Since there is no appreciable improvement by reducing the fits, there may be noise in the data or the quadratic models (both full and reduced) do not sufficiently represent the data.

Comparing the full quadratic models predictions for the training cases to the CFD results of the various objectives, the variations for Objectives-1, 2 and 4 (TF_{max} , TW_4 and X_{cc} , respectively) were found to be negligible (Figures 10a, 10b and 10d), suggesting no need for further improvement. However, a large number of points lie away from the best fit in the plot of Objective-3 (TT_{max}) (Figure 10c).

Based on this observation, a cubic model is generated for Objective-3 (TT_{max}). A full cubic fit in a 4-design variable model requires a minimum of 35 design points. To obtain a good fit, the number of design points should be considerably larger than the required number. Since there are only 38 design points available from the training set, the testing set is also included in the training set. The $PRESS_{ms}$ is used to estimate the performance of the generated RS along with the σ_a . Using the 52 design points, a full cubic was generated. The values of σ_a and $PRESS_{rms}$ were 0.0348 and 0.0598, respectively. The difference between the two measures of error is noticeable. Hence, a reduced cubic model is generated with the available design points. This improves the fit with values for σ_a and $PRESS_{rms}$ being 0.0303 and 0.0388, respectively. Table 4 compares the performance of the full quadratic and the reduced cubic models for Objective-3 (TT_{max}). The reduced cubic model is seen to perform better statistically than the quadratic model. Hence, this cubic model is used for Objective-3 (TT_{max}) in the optimization studies that follow. The RSs for all four dependent variables are shown as Equations A1-A4 in the Appendix.

Using these RSs, an optimization study is conducted to study the relationship between the independent design variables and the dependent variables that are indicators of life and performance. Also, the ability to accommodate design features that promote extended life in a design while maintaining reasonable performance is explored. Three separate examples are presented below. First, single-objective minimizations are shown. Secondly, multi-objective optimizations are performed with equal weights. Finally, the multi-objective optimizations are conducted with variable weights.

(a) Single-Objective Optimization

The purpose of this effort is twofold. First, we want to verify the performance of the optimization methodology in locating the minimum values for single objectives in the chosen design space. This verification is straightforward and necessary, but not sufficient to conclude that the technique is useful for injector design. Table 5 shows the results of optimizing (here, minimizing) each objective separately. The numbers in parentheses in Table 5 indicate the weights applied during the optimization process. Here, a weight of one means that objective was included while a weight of zero means that variable was excluded. Since the dependent variables extracted from the CFD solutions are normalized between 0 and 1 based on the generated response surfaces, the minimum value for each is necessarily 0. The optimizer found the correct value for each of the four cases.

Secondly, this process is helpful in understanding the injector operational influences via trend identification and variable groupings. The results from Table 5 are shown graphically in Figure 11 to facilitate the discussion. It was shown earlier that the flow entrained in the large recirculation zone regulated both the maximum temperature on the injector face, Objective-1 (TF_{max}) and the chamber wall temperature, Objective-2 (TW_4) (Figure 6). The results from Opt-Cases 1 and 2 support this conclusion. Minimization of Objective-1 (TF_{max}) very nearly minimizes Objective-2 (TW_4) and vice versa. Not surprisingly, the designs for the two cases are also quite similar. Both designs are shear coaxial ($Variable-1 (\alpha) = 0$) with the hydrogen flow area, $Variable-2 (\Delta HA)$, and the oxidizer post tip thickness, $Variable-4 (OPTT)$, at their maximum values. Table 5 shows that $Variable-3 (\Delta OA)$ is the only inconsistent variable in the two designs. In terms of the other dependent variables, when either Objective-1 (TF_{max}) or Objective-2 (TW_4) is minimized, the maximum oxidizer post tip temperature, Objective-3 (TT_{max}), is high. The resulting moderate-to-long combustion lengths, Objective-4 (X_{cc}), are consistent with the relatively slow mixing expected from a shear coaxial element.

Reference to Opt-Cases 3 and 4 in Table 5 and Figure 11 also suggests a correlation between Objectives-3 and 4 (TT_{max} and X_{cc} , respectively), although not as tight as the one for Objectives-1 and 2 (TF_{max} and TW_4 , respectively). When Objective-3 (TT_{max}) is minimized, Objective-4 (X_{cc}) is low and vice versa. Further investigation needs to be done to completely understand the physics that underlies this correlation. Here, both designs are impinging-like with the hydrogen flow angle, $Variable-1 (\alpha)$, at or near its maximum value and Variables-2 and 4 (ΔHA and $OPTT$, respectively) at their minimum values in the chosen design space. Again, Table 5 shows that $Variable-3 (\Delta OA)$ is the only inconsistent variable between the two cases. Both minimizations result in very high values for

Objectives-1 and 2 (TF_{max} and TW_4 , respectively). Not surprisingly, the impinging elements represented by the two designs yield significantly shorter combustion lengths than the shear coaxial designs.

The trends for Variables-1, 2 and 4 (α , ΔHA and $OPTT$, respectively) are consistent between the two pairs of dependent variables but Variable-3 (ΔOA) varies among the four cases. With the other design variables set at the design levels, Figure 12a shows the variation of Objectives-1 and 2 (TF_{max} and TW_4 , respectively) with Variable-3 (ΔOA). A similar plot for Objectives-3 and 4 (TT_{max} and X_{cc} , respectively) is shown in Figure 12b. Objective-1 (TF_{max}) is the dependent variable least sensitive to Variable-3 (ΔOA). It is also the only variable to exhibit a minimum value in the interior of the design space. This finding suggests that expanding the design space could result in more robust designs for the multi-objective optimization. The trends for Objectives-2 and 4 (TW_4 and X_{cc} , respectively) are similar to each other, with Variable-3 (ΔOA) zero for both cases. The trend for Objective-1 (TT_{max}) relative to Variable-3 (ΔOA) is opposite.

Table 5 and Figure 11 show the resulting design is different for each of the four single-objective optimizations. These results indicate that designing robust injectors demands consideration of all the independent variables together. Figure 11 clearly shows competing design trends. Thus, meeting a set of design requirements will require a compromise design.

(b) Multi-Objective Optimization

To concurrently evaluate component life and performance considerations, a multi-objective optimization study is carried out. Starting with performance (Objective-4 (X_{cc})) as most of the injector design tools do, the objectives influencing thermal environments are added one at a time to study the effect on the resulting optimum designs. These optimum designs are presented in Table 6 and Figure 13 where Opt-Case 4, with Objective-4 (X_{cc}) minimized is repeated as the starting point. Recall, the design for this case is an impinging element ($Variable-1 (\alpha) = 0.917$) with minimum flow areas and the thinnest oxidizer post tip. The consequences of this design are a minimum Objective-4 (X_{cc}), a low Objective-3 (TT_{max}) and very high values of Objectives-1 and 2 (TF_{max} and TW_4 , respectively).

When Objective-3 (TT_{max}) is minimized along with Objective-4 (X_{cc}) in Opt-Case 5, the optimum design does not change significantly from that in Opt-Case 4. The hydrogen flow angle increases from 0.917 to 1.0. The values of Variables-2, 3 and 4 (ΔHA , ΔOA and $OPTT$, respectively) all remain unchanged from Opt-Case 4. Objective-4 (X_{cc}) is unchanged as compared to Opt-Case 4, whereas Objective-3 (TT_{max}) is marginally improved from 0.181 to 0.152. The other thermal objectives remain at very high levels. Recall from Table

5 that Variable-3 (ΔOA) was 1.0 for the single-objective optimization of Objective-3 (TT_{max}). More insight regarding the optimum design can be gained by visualizing Figure 12b. Although the individual Objectives-3 and 4 (TT_{max} and X_{cc} , respectively) drive the design towards the opposite ends of the range of Variable-3 (ΔOA), the composite desirability function, D, has marginal variation with respect to Variable-3 (ΔOA). The optimizer picks the value of Variable-3 (ΔOA) that gives the maximum value of the desirability function, D. The optimum design at this point is affected mostly by the other design variables. This shows the benefits of using a global optimization procedure, which helps identify the trend of the composite function over the design space even when the individual objectives have opposing trends.

Opt-Case 6 minimizes Objective-1 (TF_{max}) simultaneously with Objectives-3 and 4 (TT_{max} and X_{cc} , respectively). In terms of the design variables, Variable-2 (ΔHA) has now shifted from 0 to 1, while the other three remain at the same values as in Opt-Case 5. This shift in Variable-2 (ΔHA) is consistent with the single-objective minimization of Objective-1 (TF_{max}) shown as Opt-Case 1 in Table 5. This single change in the design produces dramatic changes in the dependent variables. As desired, the value of Objective-1 (TF_{max}) has decreased significantly from 1.0 to 0.376. The concurrent large drop in the value of Objective-2 (TW_4) is consistent with the earlier conclusion linking Objectives-1 and 2 (TF_{max} and TW_4 , respectively). Objective-3 (TT_{max}) remains essentially unchanged. The increase in Objective-4 (X_{cc}) from 0 to 0.279 is a negative impact of the design change. Figure 14 sheds more light on the situation. Figure 14a plots the individual responses as a function of Variable-2 (ΔHA). Figure 14b is similar, with the individual responses plotted as a function of Variable-3 (ΔOA). These figures clearly illustrate that both Objectives-1 and 2 (TF_{max} and TW_4 , respectively) are considerably more sensitive to Variable-2 (ΔHA) than Variable-3 (ΔOA). Accordingly, the optimizer uses the hydrogen flow area to most efficiently regulate Objective-1 (TF_{max}). Figure 14a also shows the positive slope of Objective-4 (X_{cc}) relative to Variable-2 (ΔHA), which is responsible for the fairly large performance drop seen in this design.

Opt-Case 7 adds the final dependent variable, Objective-2 (TW_4). Table 5 shows that addition of Objective-2 (TW_4) has no effect on the design and consequently no effect on any of the dependent variables. Objective-2 (TW_4) has previously been shown to be linked with Objective-2 (TF_{max}), so this result is not surprising.

The injector design resulting from inclusion of all the dependent variables in the optimization process (Opt-Case 7) is different from Opt-Case 4 where only the performance indicator, Objective-4 (X_{cc}) was optimized.

In the design space evaluated for this effort, Variable-2 (ΔHA) has a very strong effect on the system, especially for Objectives-1 and 2 (TF_{max} and TW_4 , respectively). Reference to Figure 14 shows that at the zero value for both Variables 2 and 3 (ΔHA and ΔOA , respectively), Objective-2 (X_{cc}) is still decreasing. Performance could probably be further improved (i.e., Objective-4 (X_{cc}) shortened) by enlarging the design space to include smaller values of Variables 2 and 3 (ΔHA and ΔOA , respectively). In the process of designing a real injector, the large drop in performance affected by the consideration of Objectives-1 and 2 (TF_{max} and TW_4 , respectively) would probably require a compromise design with certain variables weighted more heavily than others.

To further probe the interplay between injector performance and component life, a composite optimization study is conducted with varying weights on the individual objective functions embodied by the composite desirability function. This is a functionality that the new design optimization methodology must possess. The designer must be able to weight, or favor, one or more dependent variables to have maximum flexibility in addressing design requirements. The results of this part of the study are shown in Table 7 and Figure 15. Reference to Table 7, where the numbers in parenthesis indicate the weight in the composite desirability function for that variable, shows that the designs suggested by Opt-Case 8 and Opt-Case 10 are similar. In Opt-Case 8 the life influencing variables (Objectives-1, 2 and 3 (TF_{max} , TW_4 , and TT_{max} , respectively)) are weighted by a 2:1 ratio over the performance indicator (Objective-4 (X_{cc})). Opt-Case 10 is the opposite, with performance having a 2:1 weighting over the life variables. Reference to Tables 6 and 7 shows that the design variables and dependent variables for these two cases are almost identical to those in Opt-Case 7, where all four variables are weighted equally. Figure 14b shows the composite desirability function D, for Opt-Case 7, to be reasonably flat as a function of Variable-3 (ΔOA). Thus, small weightings have little or no effect on the injector design.

The other two cases shown in Table 7, Opt-Case 9 and Opt-Case 11, have relative weightings of 50:1 and 1:50, respectively for life (Objectives-1, 2 and 3, (TF_{max} , TW_4 , and TT_{max} , respectively)) and performance indicators (Objective-4 (X_{cc})). For Opt-Case 9, the design tends toward the cases where Objectives-1 and 2 (TF_{max} and TW_4 , respectively) were individually minimized. The exception is that Variable-4 (OPTT) is equal to zero, which is required to minimize Objective-3 (TT_{max}). For Opt-Case 11, the resulting design tends toward Opt-Case 4 where Objective-4 (X_{cc}) is minimized. Even with this strong weighting, the effect of including Objectives-1 and 2 (TF_{max} and TW_4 , respectively) is felt with the value of Variable-1 (α)

equal to 0.612. When Objective-4 (X_{cc}) is minimized by itself, Variable-1 (α) is equal to 0.917.

Figure 16 shows the joint desirability function, D, for Opt-Case 9 (with a weighting of 50:1 in favor of life over performance), to be fairly flat. Accordingly, small weightings have little effect on the design. Significant weightings must be applied to push the design very far toward either life or performance. Opt-Case 11 has good performance and a low injector tip temperature. However, the chamber wall and injector face temperatures are very high. In an actual design, if this level of performance was required, active cooling could be required for the chamber wall and injector face.

Additional CFD solutions were executed to confirm the optimum designs obtained from RS for all 11 Opt-Cases. These results are shown in Tables 5, 6 and 7. The dependent variable error, as defined by Equation 8, is also shown for each case. The error is on the order of four percent or less in the case of Objective-3 (TT_{max}). The error for the other three dependent variables is less than one percent. The larger discrepancy in Objective-3 (TT_{max}) is likely due to the steady state assumption made in the CFD analyses for this effort. The injector problem is actually unsteady.

4. SUMMARY AND CONCLUSIONS

In this study, a demonstration of a CFD-based design optimization methodology for a single element rocket injector is presented. The design variables indicating the thermal environment and performance of the element are identified and the design points selected using a DOE technique. CFD computations are carried out for each design and appropriate orders of polynomial-based response surfaces are generated for the estimated objectives. Based on the performance of the RS a grid refinement study is carried out and a new, more efficient grid is generated. Utilizing the results obtained from CFD computations on the fine grid, an optimization study is carried out and correlations between different objectives are identified. Relationships between the dual goals of performance and life are evaluated in depth.

The conclusions from this work fall into two broad categories. First, general conclusions can be made concerning the design optimization process itself and its relationship to the quality of the CFD solutions, its implications for code validation and its potential impact on injector design. Second, more specific observations can be drawn based on the injector design. General conclusions based on the design optimization process include the following:

- The degree of spread of a dependent variable over a parametric space is an important criterion for validation experiment design. Evaluation of large parametric spaces provides insight into potential validation measurements

- Correlations of the variables highlight the trends and provide insight into physical processes that regulate the dependent variables.
- The study confirms that the details of the injector design govern the performance. As stated in Ref. 8, directing the fuel flow towards the element axis and thinning the oxidizer post lead to better performance. The same details are shown to have a large impact on the injector and combustion chamber environmental variables as well.
- Using CFD to evaluate and include more independent and dependent variables in the conceptual design phase has potential to create more robust designs. This increase in the dimensionality of the design problem also creates the requirement for an optimization tool to guide the designer through often opposing trends to an acceptable design compromise.
- In the context of this study, the proposed RSM worked well. It was fairly efficient in terms of the number of CFD solutions required and provided sensible results in view of the physics of the problem.
- Although more work needs to be done, the new methodology appears to have promise in helping injector designers address the NGLT goals. The current study has established the need of addressing conflicting design goals early in the design process.
- For both single- and multi-objective optimization efforts, in many cases, the resultant designs are at an extreme of the design space. This indicates the design space could be enlarged subject to practical design considerations. Again, a merit of the RSM is that the solutions obtained can be used repeatedly when revising the design scope. Furthermore, different scenarios, with either single- or multi-objective optimization, can make use of the information supplied by the response surface repeatedly.

More specific observations based on the injector design applications include the following:

Single-Objective Optimization

- The optimizer reliably locates single variable minimum values.
- Minimization of the individual dependent variables yields a different injector design for each variable minimized. This establishes the fact that designing an efficient long life injector requires concurrent evaluation of all the relevant design variables.
- For the current study:
 1. The four design objectives, based on the design obtained during their individual minimization, largely fall into two groups: Objectives-1 and 2 (TF_{max} and TW_4 , respectively) and Objectives-3 and 4, (TT_{max} and X_{cc} , respectively). However,

- there are differences between them. In each group, the responses of the two design objectives to Variable-3 (ΔOA) are different. The observation also indicates that the three life-related objectives require compromises between design variables.
2. Minimizing Objectives-1 and 2 (TF_{max} & TW_4 , respectively) leads to a design with Variable-1 (α) equal to zero (shear coaxial element), maximum fuel flow area and thickest post tip. This design also yields moderate to poor performance due to the slow mixing across the shear layer.
 3. Minimizing Objectives-3 and 4 (TT_{max} and X_{cc} , respectively) results in an impinging-like design with Variable-1 (α) equal to one. It also has the minimum fuel flow area and the thinnest post tip thickness. This design performs well, but has very high wall and injector face temperatures.

Multi-Objective Optimization

- The injector design, when multiple dependent variables are included, is different from any of the single variable minimizations. For example, although the individual objectives, Objectives-3 and 4 (TT_{max} and X_{cc} , respectively), drive the design towards the opposite ends of the range of Variable-3 (ΔOA), the composite desirability function accounting for all their effects exhibits only marginal variation with respect to Variable-3. The optimum design is affected mostly by other design variables.
- One can clearly see the benefit of using a global optimization procedure, which helps identify and interpret the trend of the composite function over the design space, especially when the individual objectives have opposing patterns.

For the current study the following specific observations can be made:

1. Equal weights
 - a) The design with all 4 dependent variables included (Opt-Case 7) is still an impinging element with low to moderate temperatures, but marginal performance.
 - b) Figure 14 indicates that lowering either propellant flow area beyond the current limit would probably decrease Objective-4 (X_{cc}) and thus increase performance. Lowering the oxidizer area would probably have less adverse effect on Objectives-1 and 2 (TF_{max} & TW_4 , respectively)
2. Unequal weights
 - a) This capability is required to find acceptable designs
 - b) With modest weights on either the performance (Objective-4 (X_{cc})) or life

(Objectives-1, 2 and 3 (TF_{max} , TW_4 and TT_{max} respectively)), the design does not change appreciably.

- c) Opt-Case 11 (with a large emphasis on performance) gives very good performance, modest Objective-3 (TT_{max}), but very high values of Objectives-1 and 2 (TT_{max} and TW_4 , respectively). If enlarging the design space does not help, active cooling may be required.

5. ACKNOWLEDGEMENTS

This study has been supported in part by NASA Marshall Space Flight Center. The authors would also like to acknowledge Dr. Raphael T. Haftka for his valuable suggestions.

6. REFERENCES

1. Rupe, J. H., "An Experimental Correlation of the Nonreactive Properties of Injection Schemes and Combustion Effects in a Liquid Rocket Engine," NASA TR 32-255, 1965.
2. Pieper, J. L., "Oxygen/Hydrocarbon Injector Characterization," PL-TR 91-3029, October 1991.
3. Nurick, J. H., "DROP MIX - A PC Based Program for Rocket Engine Injector Design," JANNAF Propulsion Conference, Cheyenne, Wyoming, 1990.
4. Dickerson, R., Tate, K., Nurick, W., "Correlation of Spray Injector Parameters with Rocket Engine Performance," AFRPL-TR-68-11, January 1968.
5. Pavli, A. L., "Design and Evaluation of High Performance Rocket Engine Injectors for Use with Hydrocarbon Fuels," NASA TM 79319, 1979.
6. Calhoon, D., F. Ito, J. I. and Kors, D. L., "Investigation of Gaseous propellant Combustion and Associated Injector-Chamber Design Guidelines," Aerojet liquid rocket company, NASA Cr-121234, Contract NAS3-13379, July 1973.
7. Cheng, G.C., and Farmer, R.C., "CFD Spray Combustion Model for Liquid Rocket Engine Injector Analyses," AIAA Paper 2002-0785, 40th AIAA Aerospace Sciences Meeting & Exhibit, Jan. 14-17, 2002.
8. Gill, D. S. and Nurick, W. H., "Liquid Rocket Engine Injectors," NASA SP-8089, NASA Lewis Research Center, March, 1976.
9. Myers, R. H., and Montgomery, D. C., *Response Surface Methodology – Process and Product Optimization Using Designed Experiment*, John Wiley & Sons, 1995.
10. JMP[®] Design of Experiments, Version 5, Copyright © 2002, SAS Institute Inc., Cary, NC, USA.
11. Calhoon, D. F., Ito, J. I. and Kors, D. L., "Handbook for Design of Gaseous Propellant Injectors and Combustion Chambers," 1973.

12. Chen, Y. S., "Compressible and Incompressible Flow Computation with a Pressure-Based Method," AIAA89-0286, AIAA 28th Aerospace Sciences Meeting, January 9-12, 1989.
13. Wang, T. S. and Chen, Y. S., "A United Navier-Stokes Flowfield and performance Analysis of Liquid Rocket Engines," AIAA 90-2494, AIAA 26th Joint Propulsion Conference, July 16-18, 1990.
14. Chen, Y. S. and Farmer, R. C., "CFD Analysis of Baffle Flame Stabilization," AIAA 91-1967, AIAA 27th Joint Propulsion Conference, June 24-26, 1991.
15. Owen, A., "Orthogonal Arrays for: Computer Experiments, Integration and Visualization," Statistica Sinica, Vol. 2, No.2, pp. 439-452, 1992.
16. Shyy, W., Papila, N., Vaidyanathan, R. and Tucker, K., Global Design Optimization for Aerodynamics and Rocket Propulsion Components, *Progress in Aerospace Sciences*, Vol. 37 (2001), pages 59-118
17. Papila, N. U., Neural Network and Polynomial-Based Response Surface Techniques or Supersonic Turbine Design Optimization, PhD Dissertation, University of Florida, 2001.
18. Mullin, M. and Sukthankar, R., "Complete Cross-Validation for Nearest Neighbor Classifiers," 17th International Conference on Machine Learning (ICML), Stanford, California, 2000.
19. JMP™, The Statistical Discovery Software™, Version 5, Copyright © 1989-2002, SAS Institute Inc., Cary, NC, USA.
20. Allen, D. M., "Mean Square Error of Prediction as a Criterion for Selecting Variables," *Technometrics*, 13, pages 469-475, 1971.
21. Allen, D. M., "The Relationship Between Variable Selection and Data Augmentation and a Method for Prediction," *Technometrics*, 16, pages 125-127, 1974.
22. Microsoft→ Excel 2000, Copyright © 1985-1999, Microsoft Corporation, Seattle, WA.
23. Lasdon, L.S., Waren, A., Jain, A., and Ratner, M., "Design and Testing of a Generalized Reduced Gradient Code for Nonlinear Programming," *ACM Transactions on Mathematical Software* 4:1, 1978.

Variable	Minimum		Maximum	
	Actual	Normalized	Actual	Normalized
α	0°	0	α^o	1
ΔHA	Baseline	0	Baseline+25%	1
ΔOA	Baseline-40%	0	Baseline	1
$OPTT$	x in	0	2x in	1

Table 1: Range of design variables (α is an acute angle in degrees and x is the thickness of OPTT in inches)

Case	α	ΔHA	ΔOA	$OPTT$	TF_{max}	TW_4	TT_{max}	X_{cc}
X	1	0	0	0	0.998	0.927	0.128	-0.004
Y	0	0.5	0.5	1	0.285	0.395	0.923	0.567

Table 2. Independent and dependent variable (Objectives) for Cases X and Y from CFD computations
{Normalized values shown}.

		Full quadratic RS	Reduced quadratic model
TF_{max}	Number of observations	38	38
	σ_a	0.00566	0.00546
	σ (14 points)	0.00460	0.00463
	Mean	0.495	
TW_4	Number of observations	38	38
	σ_a	0.00803	0.00795
	σ (14 points)	0.00669	0.00799
	Mean	0.514	
TT_{max}	Number of observations	38	38
	σ_a	0.0413	0.0401
	σ (14 points)	0.0396	0.0382
	Mean	0.560	
X_{cc}	Number of observations	38	38
	σ_a	0.0205	0.0197
	σ (14 points)	0.0178	0.0186
	Mean	0.497	

Table 3: Performance of full and reduced quadratic RSs for the four objective functions {Non-normalized values used}.

		Full quadratic RS	Reduced cubic RS
TT_{max}	Number of observations	38	52
	σ_a	0.0413	0.0303
	PRESS _{ms}	0.0521	0.0388
	Mean	0.560	0.591

Table 4: Performance of RSs for the TT_{max} . Reduced cubic RS has 21 coefficients {Non-normalized values used}.

Opt-Case	α	ΔHA	ΔOA	OPTT	TF_{max}	TW_4	TT_{max}	X_{cc}
1	0	1	0.592	1	0.0 (1)	0.0725 (0)	0.914 (0)	0.769 (0)
CFD					-0.00207	0.0656	0.936	0.758
error (%)					0.11	0.08	0.70	0.25
2	0	1	0	1	0.0309 (0)	0.0 (1)	1.0 (0)	0.440 (0)
CFD					0.091	0.0461	0.911	0.568
error (%)					0.90	0.57	2.84	2.93
3	1	0	1	0	0.944 (0)	0.976 (0)	0.0 (1)	0.153 (0)
CFD					0.943	0.969	0.103	0.158
error (%)					0.01	0.08	4.46	0.12
4	0.917	0	0	0	0.987 (0)	0.926 (0)	0.182 (0)	0.0 (1)
CFD					0.981	0.919	0.119	-0.004
error (%)					0.08	0.08	2.69	0.12

Table 5: Minimizing individual objectives. Value in parenthesis (1) indicates which objective function is minimized {Normalized values shown}.

Opt-Case	α	ΔHA	ΔOA	OPTT	TF_{max}	TW_4	TT_{max}	X_{cc}
4	0.917	0	0	0	0.987 (0)	0.926 (0)	0.182 (0)	0.0 (1)
CFD					0.981	0.919	0.119	-0.004
error (%)					0.08	0.08	2.69	0.12
5	1	0	0	0	1.0 (0)	0.928 (0)	0.151 (1)	0.00097 (1)
CFD					0.998	0.927	0.128	-0.004
error (%)					0.03	0.01	1.00	0.14
6	1	1	0	0	0.376 (1)	0.224 (0)	0.155 (1)	0.279 (1)
CFD					0.369	0.214	0.252	0.264
error (%)					0.10	0.12	3.93	0.38
7	1	1	0	0	0.376 (1)	0.224 (1)	0.155 (1)	0.279 (1)
CFD					0.369	0.214	0.252	0.264
error (%)					0.10	0.12	3.93	0.38

Table 6: Study of effect of life on performance. Value in parenthesis indicates the weighting on the objective functions {Normalized values shown}.

Opt-Case	α	ΔHA	ΔOA	OPTT	TF_{max}	TW_4	TT_{max}	X_{cc}
8	1	1	0.192	0	0.346 (1)	0.210 (1)	0.163 (1)	0.334 (0.5)
CFD					0.343	0.200	0.185	0.326
error (%)					0.04	0.12	0.91	0.22
9	0	1	0.497	0	0.0451 (5)	0.0823 (5)	0.471 (5)	0.627 (0.1)
CFD					0.0401	0.0767	0.404	0.613
error (%)					0.08	0.07	2.53	0.32
10	1	1	0	0	0.376 (0.5)	0.224 (0.5)	0.155 (0.5)	0.279 (1)
CFD					0.369	0.214	0.252	0.264
error (%)					0.10	0.12	3.93	0.38
11	0.612	0	0	0	0.919 (0.1)	0.898 (0.1)	0.282 (0.1)	0.0132 (5)
CFD					0.911	0.890	0.361	0.0070
error (%)					0.10	0.09	3.10	0.16

Table 7: Study of influence of life and performance objectives on each other. Value in parenthesis indicates the weighting on the objective functions {Normalized values shown}.



Figure 1: Schematic of Hybrid Boeing Element (U. S. Patent 6253539)

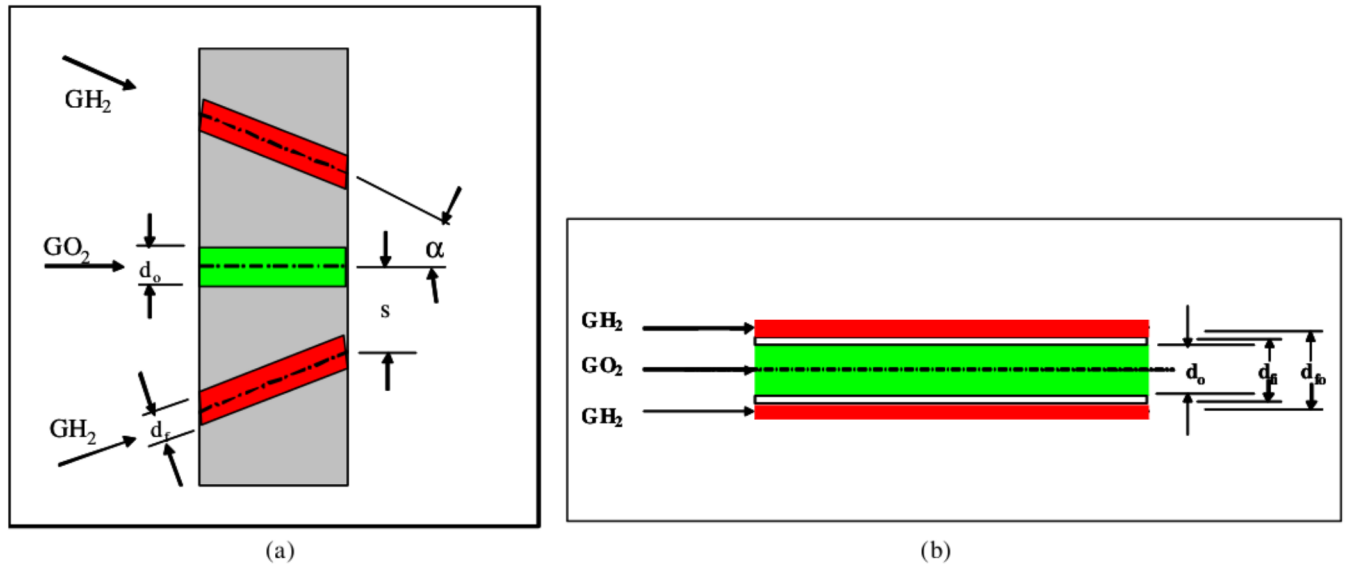
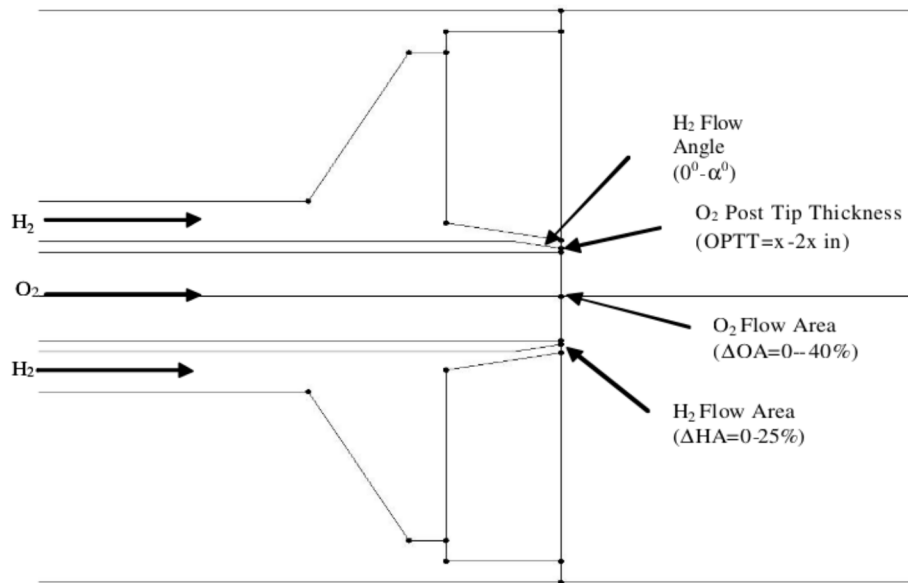
Figure 2: Schematic of the GO_2/GH_2 impinging and coaxial injector elements. (a) F-O-F impinging element, (b) coaxial element.

Figure 3: (a) Design variables and their range.

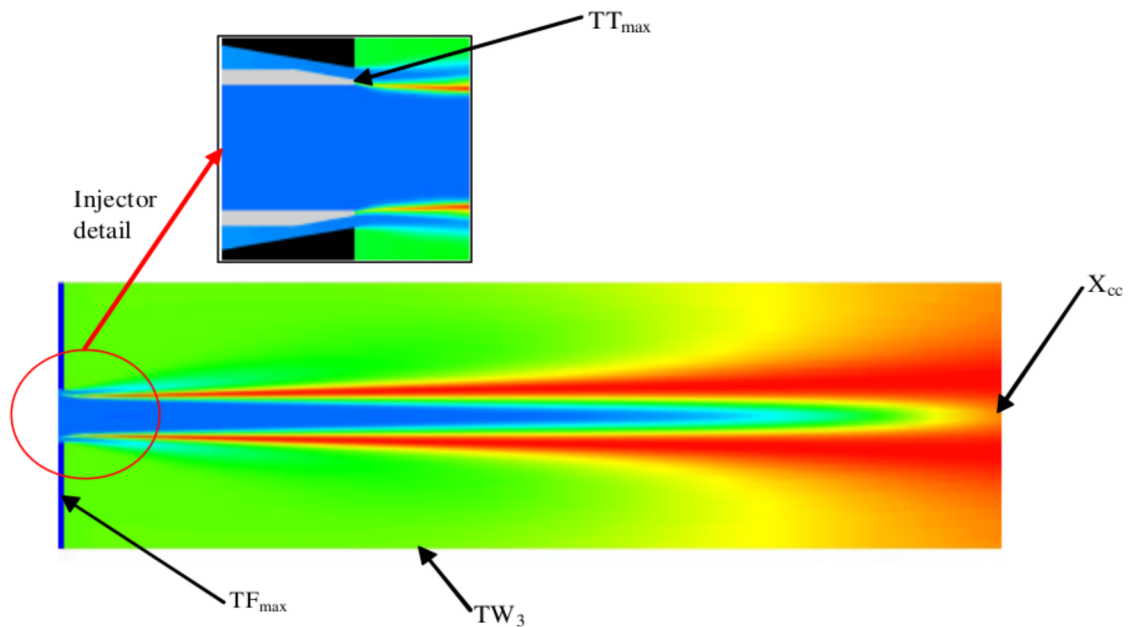


Figure 3: (b) Objective functions.

Figure 3: Design variables and objectives of the present injector optimization exercise

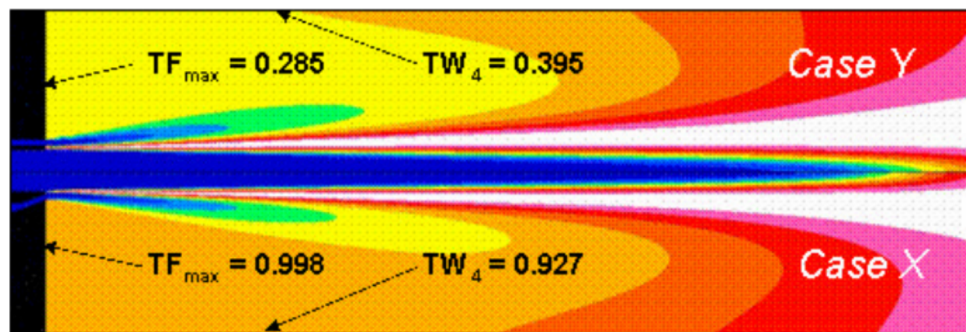


Figure 4: Temperature Field for Cases X and Y.

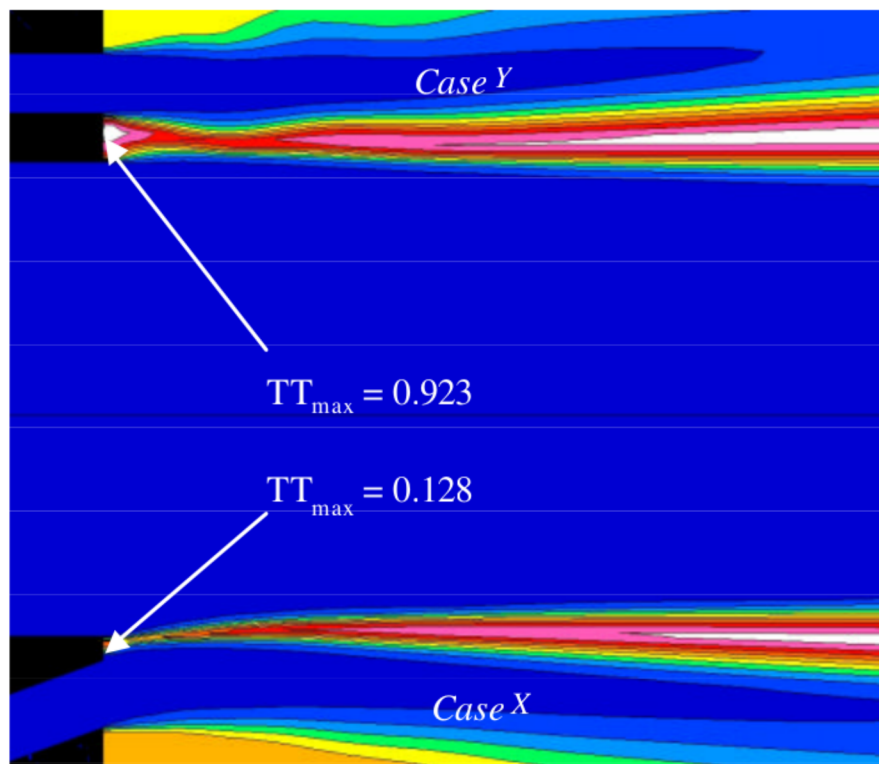


Figure 5: Near-Injector Temperature Field for Cases X and Y.

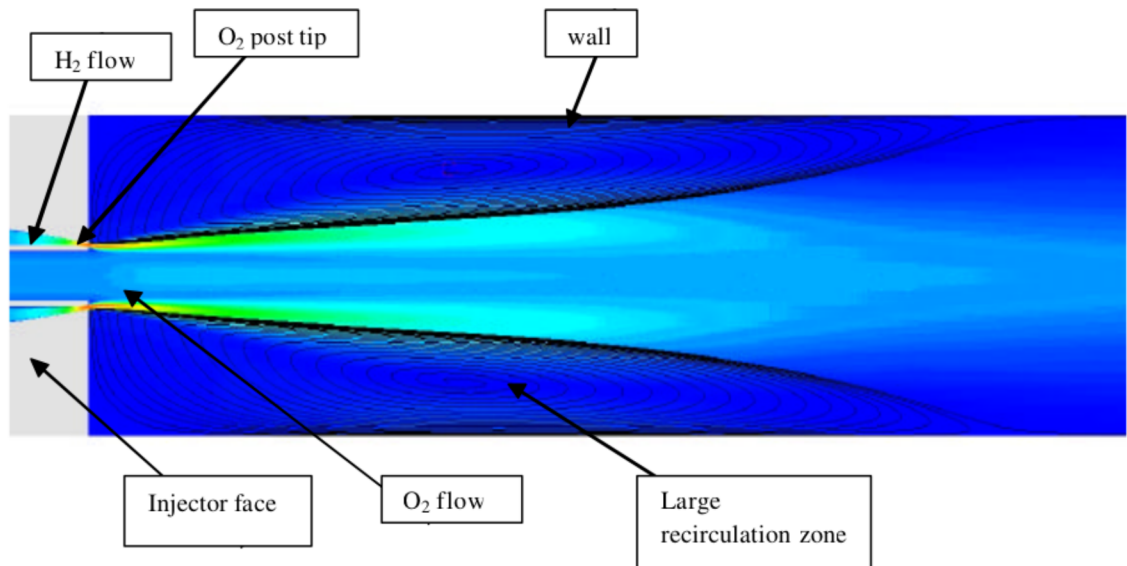


Figure 6: Large recirculation zone in the combustion chamber.

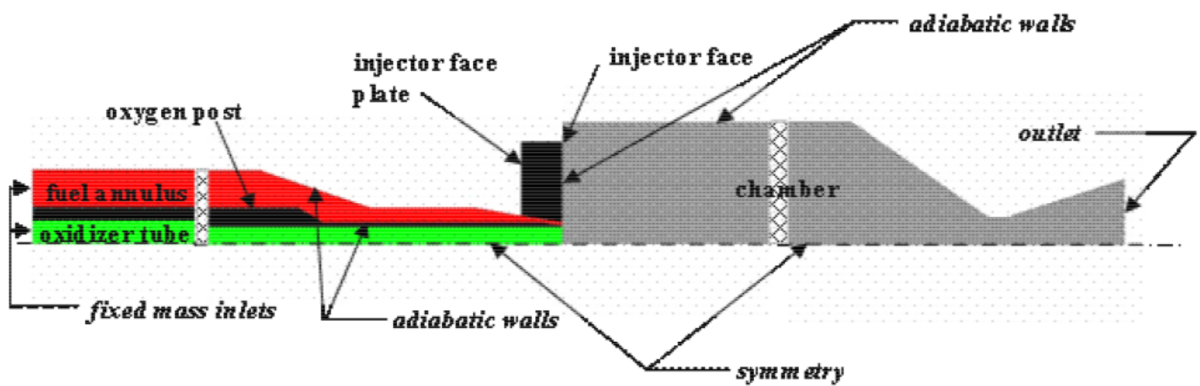


Figure 7: Simulation domain and boundary conditions

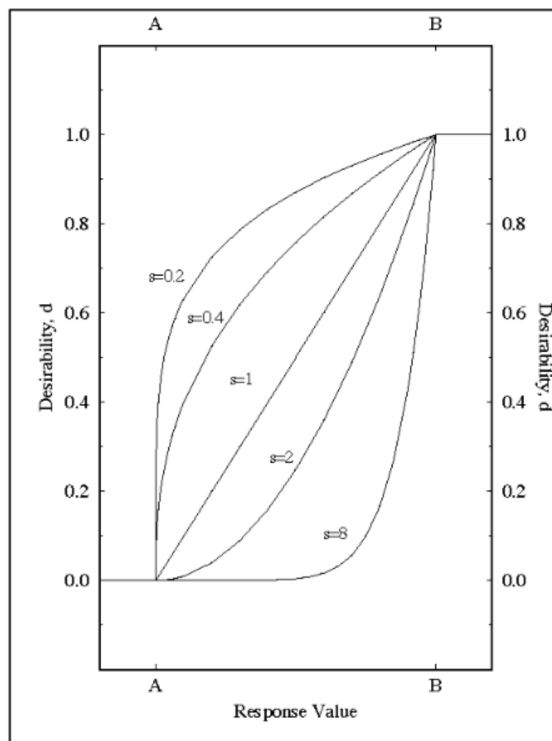
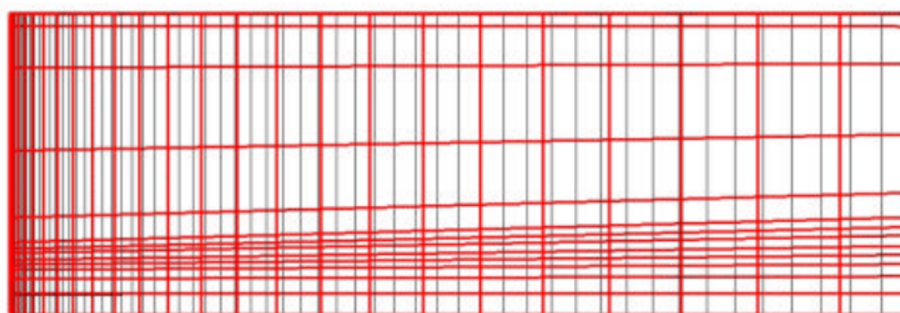
Figure 8: Desirability function (d) for various weight factors, s . (Note: $B < A$)⁹

Figure 9: Comparing the unrefined (336·81) {thicker lines} and refined (430·81) {thinner lines} grids.

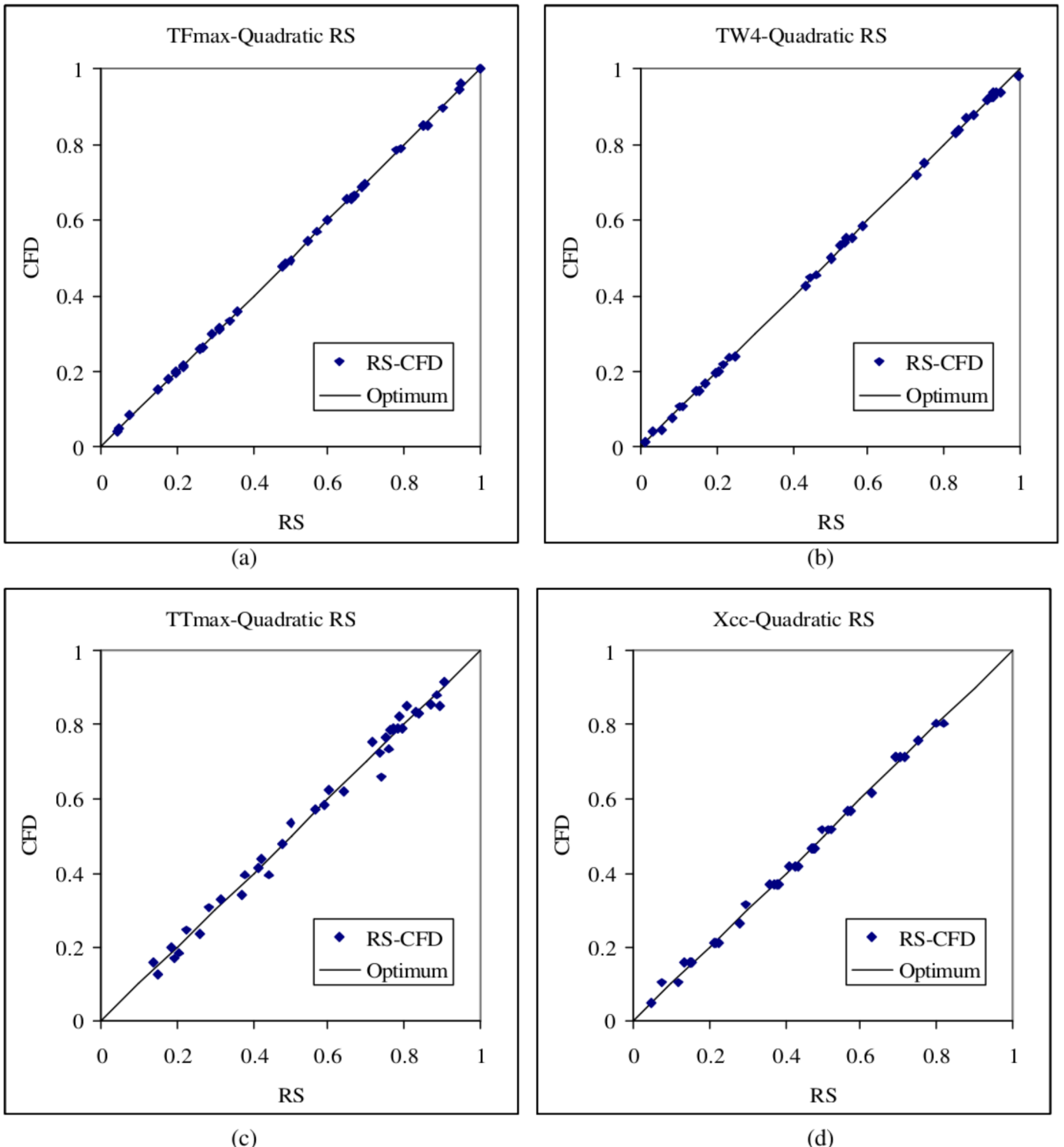


Figure 10: Comparison between the best fit possible and as predicted by quadratic response surface (a) TF_{\max} , (b) TW_4 , (c) TT_{\max} and (d) X_{cc} . Optimum refers to the case when RS and CFD values are identical. RS-CFD represents the value as for the current case (Normalized values shown).

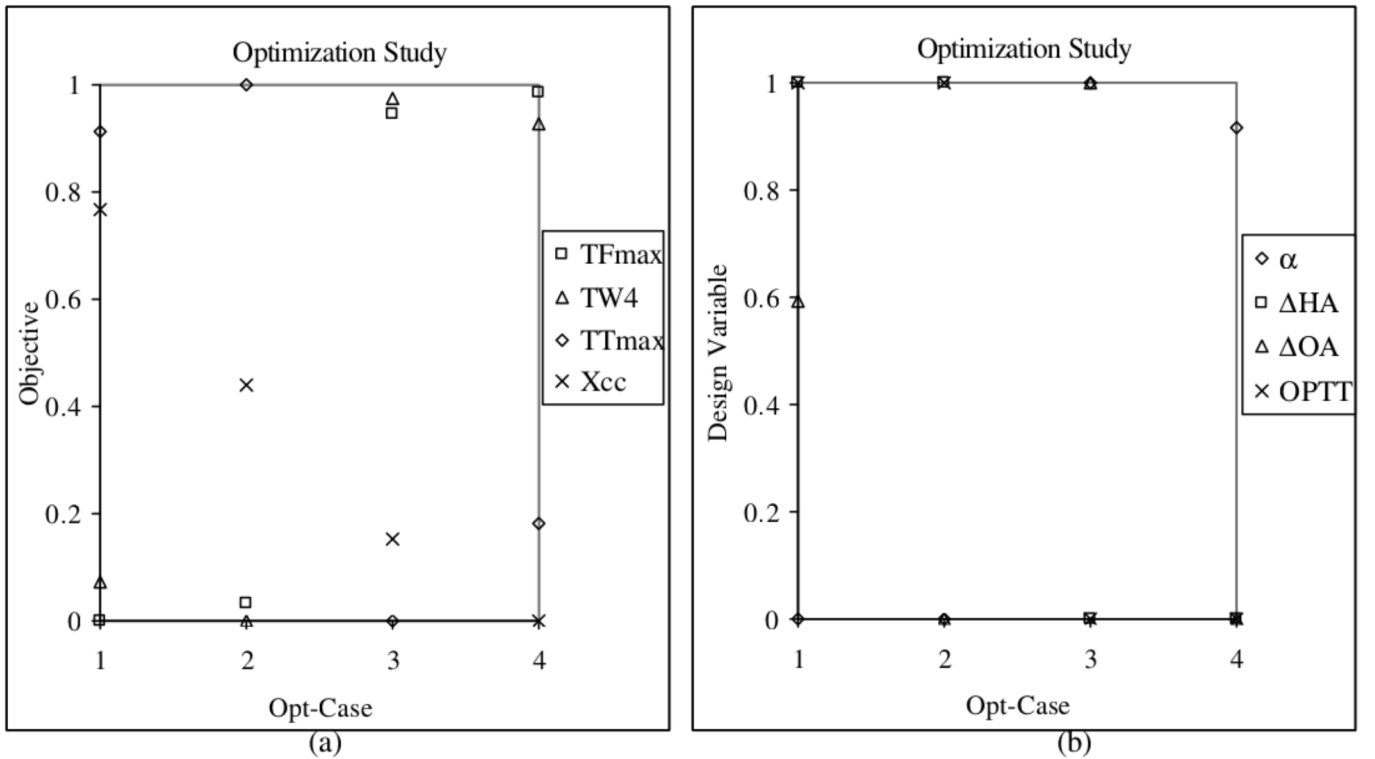


Figure 11: Minimization of different objectives. (Case 1: TF_{\max} , Case 2: TW_4 , Case 3: TT_{\max} , Case 4: X_{cc})
(a) Objectives, (b) Design Variables {Normalized values shown}.

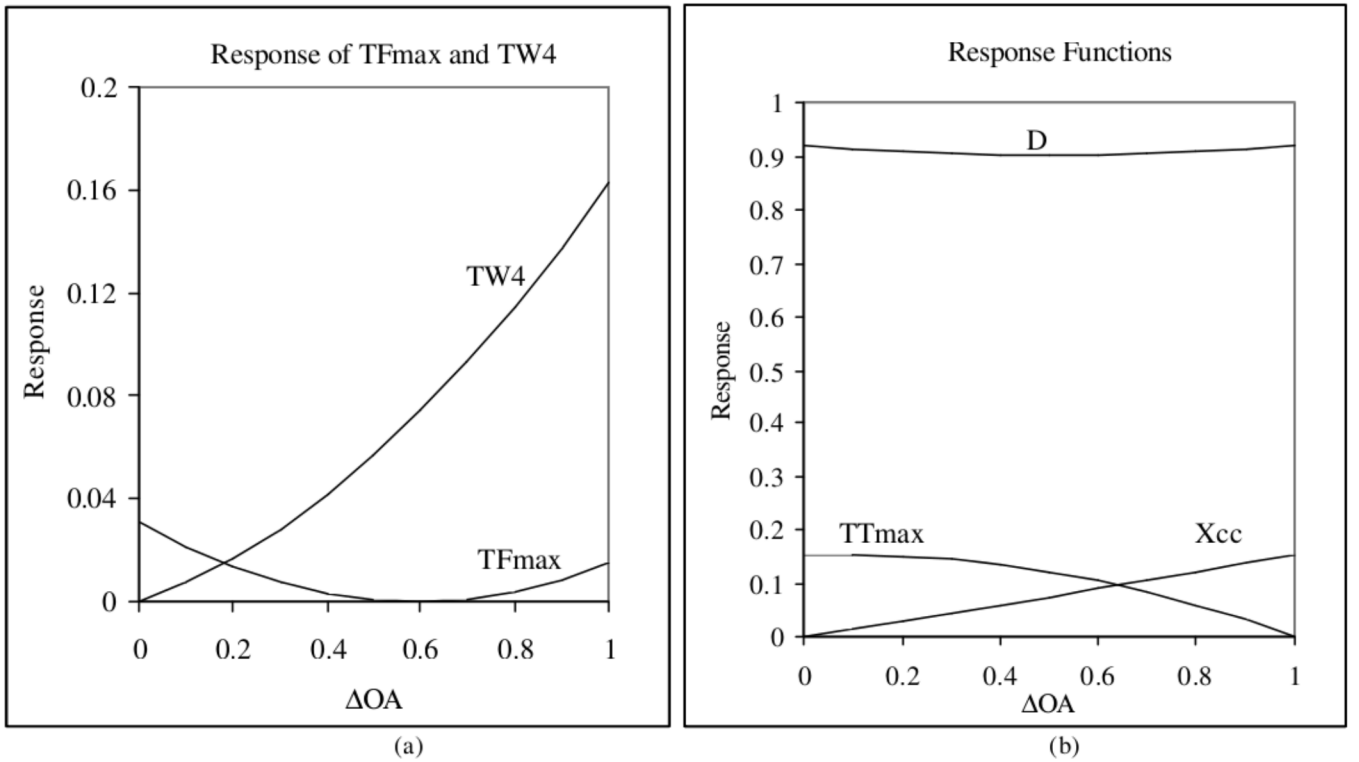


Figure 12: Variation of (a) TF_{\max} and TW_4 for $\alpha=0$, $\Delta H_A=1$ and $\text{OPTT}=1$, (b) TT_{\max} and X_{cc} for $\alpha=1$, $\Delta H_A=0$ and $\text{OPTT}=0$, with respect to ΔO_A {Normalized values shown and D is the desirability function} (all objectives are equally weighed in the composite function).

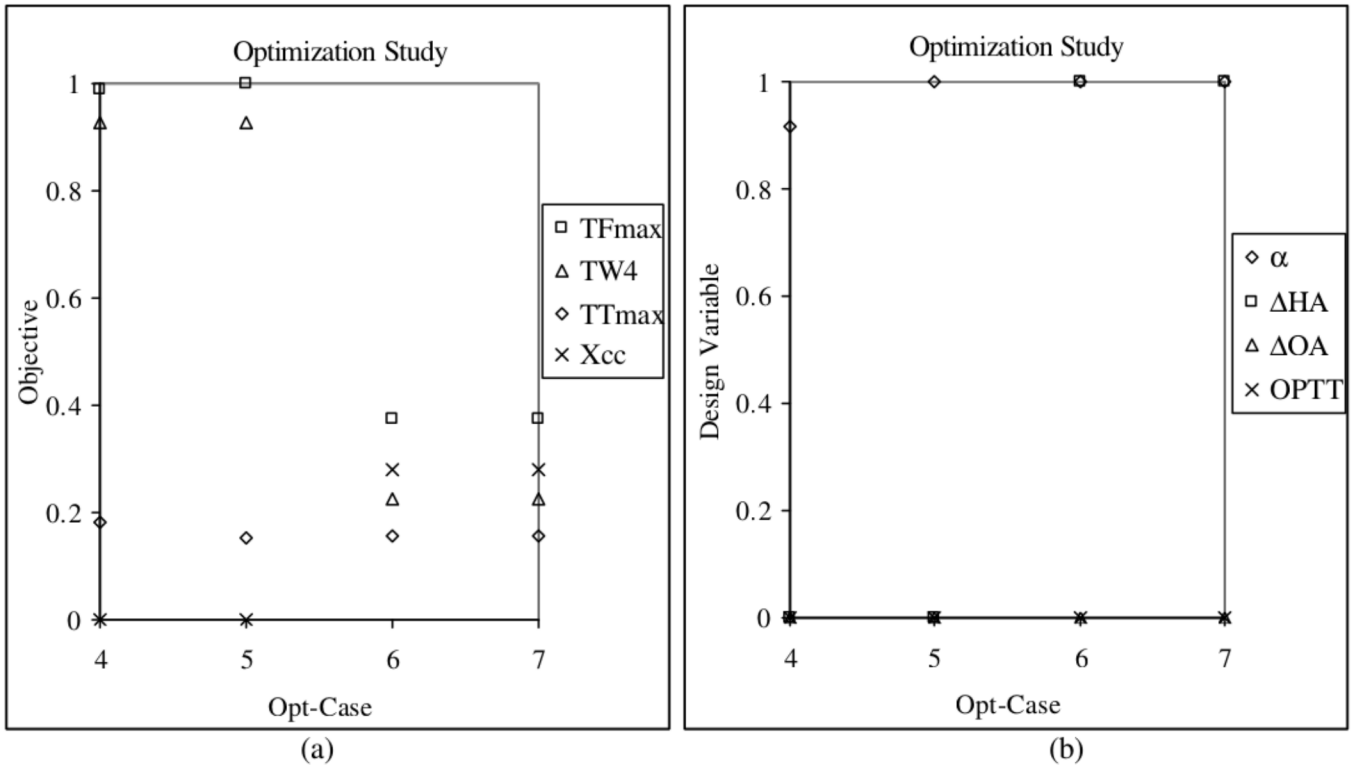


Figure 13: Composite minimization of objectives with different weightings. (Case 4: (0,0,0,1), Case 5: (0,0,1,1), Case 6: (1,0,1,1), Case 7: (1,1,1,1)) {The values in parenthesis indicates weights for (TF_{max}, TW₄, TT_{max}, X_{cc})},
(a) Objectives, (b) Design Variables {Normalized values shown}.

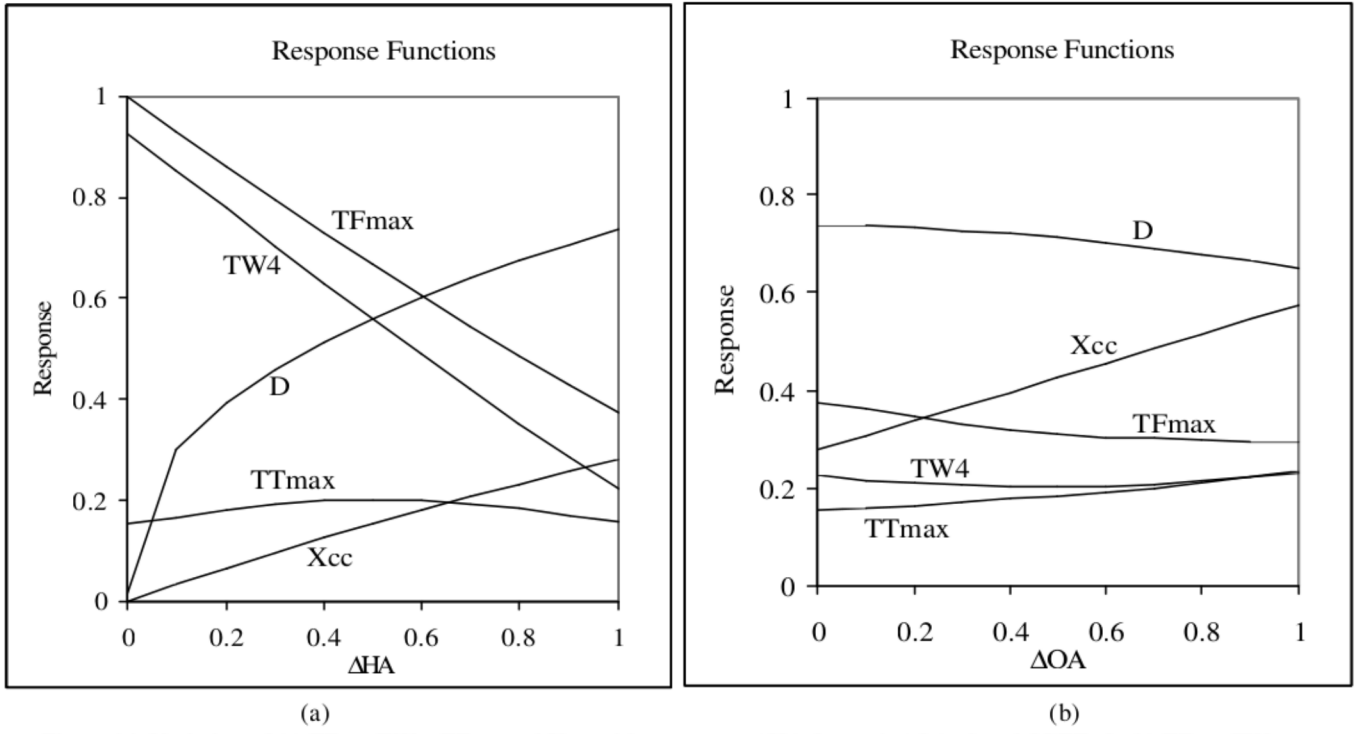


Figure 14: Variation of (a) TF_{max}, TW₄, TT_{max} and X_{cc}, with respect to Δ H_A for $\alpha=1$, Δ O_A=0 and OPTT=0, (b) TF_{max}, TW₄, TT_{max} and X_{cc}, with respect to Δ O_A for $\alpha=1$, Δ H_A=1 and OPTT=0 {Normalized values shown and D is the desirability function} (all objectives are equally weighed in the composite function).

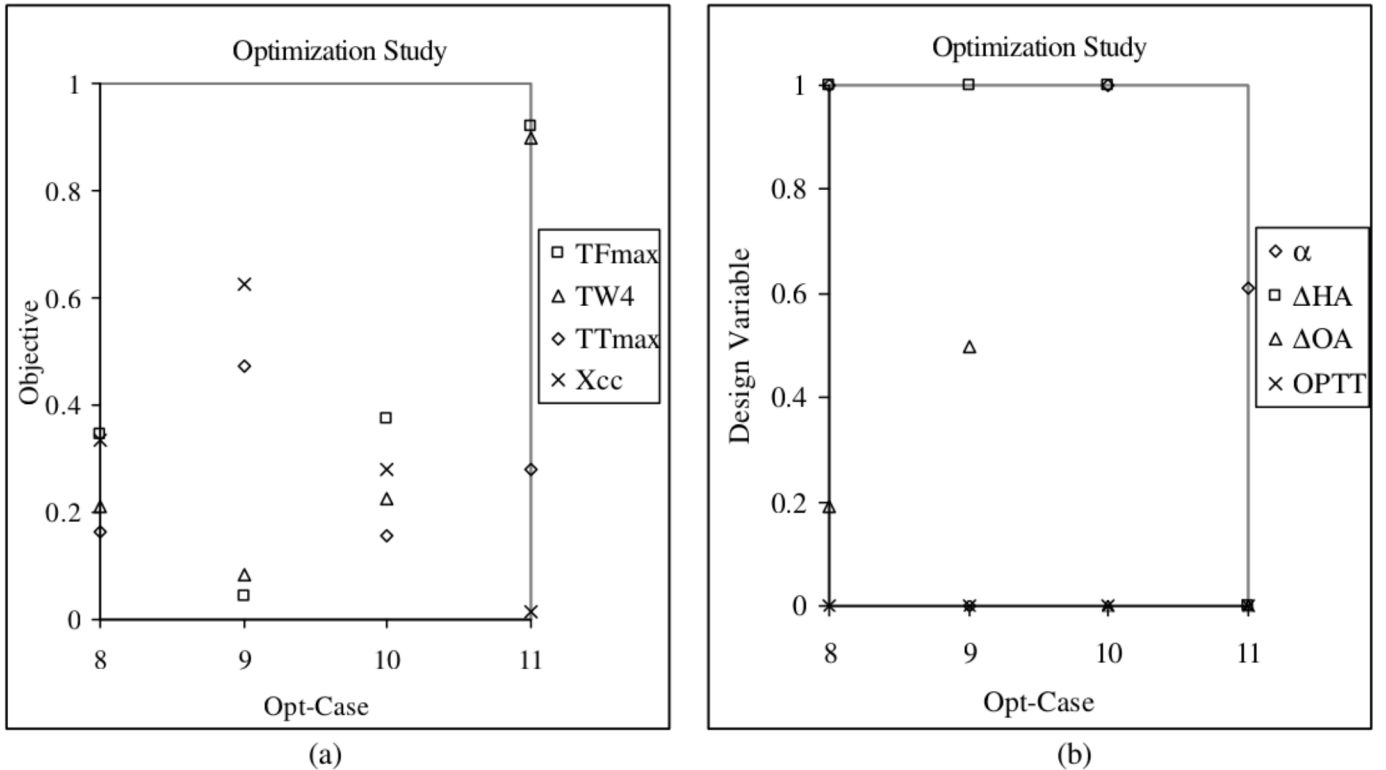


Figure 15: Composite minimization of objectives with different weightings. (Case 8: (1,1,1,0.5), Case 9: (5,5,5,0.1), Case 10: (0.5,0.5,0.5,1), Case 11: (0.1,0.1,0.1,5)) {The values in parenthesis indicates weights for (TF_{max} , TW_4 , TT_{max} , X_{cc})}, (a) Objectives, (b) Design Variables {Normalized values shown}.

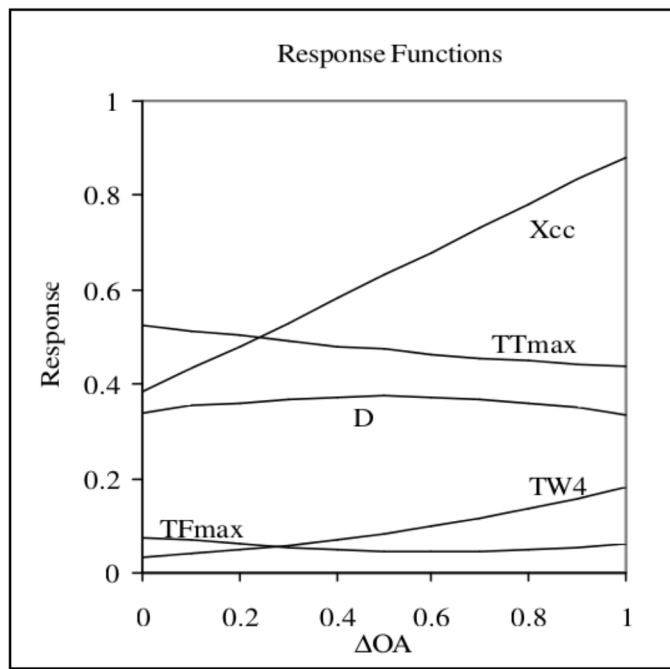


Figure 16: Variation of TF_{max} , TW_4 , TT_{max} and X_{cc} , with respect to ΔOA for $\alpha=0$, $\Delta HA=1$ and $OPTT=0$ {Normalized values shown and D is the desirability function} (Case 9: Temperatures weighted over performance in the ratio of 50:1).

APPENDIX

	H_2 flow angle (α)	Change in H_2 flow Area (ΔHA)	Change in O_2 flow Area (ΔOA)	O_2 post tip thickness (OPTT)
Case 1:	0	0	1	0
Case 2:	0	0	1	0.5
Case 3:	0	0	1	1
Case 4:	0.5	0.5	0	1
Case 5:	1	1	0.5	0
Case 6:	1	1	0.5	0.5
Case 7:	1	1	0.5	1
Case 8:	0	0.5	0.5	0
Case 9:	0.5	1	1	0
Case 10:	0.5	1	1	0.5
Case 11:	0.5	1	1	1
Case 12:	1	0	0	0
Case 13:	1	0	0	0.5
Case 14:	1	0	0	1
Case 15:	0	1	0	0
Case 16:	0	1	0	0.5
Case 18:	0.5	0	0.5	0
Case 19:	0.5	0	0.5	1
Case 20:	1	0.5	1	0
Case 21:	1	0.5	1	0.5
Case 22:	1	0.5	1	1
Case 23:	0	1	0.5	0
Case 24:	0	1	0.5	1
Case 25:	0.5	0	1	0
Case 26:	0.5	0	1	1
Case 27:	1	0.5	0	0
Case 28:	1	0.5	0	1
Case 29:	0	0	0	0
Case 30:	0	0	0	0.5
Case 32:	0.5	0.5	0.5	0.5
Case 33:	1	1	1	0
Case 34:	1	1	1	1
Case 35:	0	0.5	1	0
Case 36:	0	0.5	1	1
Case 37:	0.5	1	0	0
Case 38:	0.5	1	0	1
Case 39:	1	0	0.5	0
Case 40:	1	0	0.5	1

Table A1a: Training data (missing Case numbers indicate the unacceptable Cases).

	α	ΔHA	ΔOA	OPTT
Case 41:	0.5	0.5	0	0
Case 42:	0.5	0.5	0	0.5
Case 43:	0	0.5	0.5	0.5
Case 44:	0	0.5	0.5	1
Case 45:	0.5	0	0.5	0.5
Case 46:	0	1	0.5	0.5
Case 47:	0.5	0	1	0.5
Case 48:	1	0.5	0	0.5
Case 49:	0.5	0.5	0.5	0
Case 50:	0.5	0.5	0.5	1
Case 51:	1	1	1	0.5
Case 52:	0	0.5	1	0.5
Case 53:	0.5	1	0	0.5
Case 54:	1	0	0.5	0.5

Table A1b: Testing data.

$$TF_{max} = 0.692 + 0.477(\alpha) - 0.687(\Delta HA) - 0.080(\Delta OA) - 0.0650(OPTT) - 0.167(\alpha)^2 - 0.0129(\Delta HA)(\alpha) + 0.0796(\Delta HA)^2 - 0.0634(\Delta OA)(\alpha) - 0.0257(\Delta OA)(\Delta HA) + 0.0877(\Delta OA)^2 - 0.0521(OPTT)(\alpha) + 0.00156(OPTT)(\Delta HA) + 0.00198(OPTT)(\Delta OA) + 0.0184(OPTT)^2. \quad (A1)$$

$$TW_4 = 0.758 + 0.358(\alpha) - 0.807(\Delta HA) + 0.0925(\Delta OA) - 0.0468(OPTT) - 0.172(\alpha)^2 + 0.0106(\Delta HA)(\alpha) + 0.0697(\Delta HA)^2 - 0.146(\Delta OA)(\alpha) - 0.0416(\Delta OA)(\Delta HA) + 0.102(\Delta OA)^2 - 0.0694(OPTT)(\alpha) - 0.00503(OPTT)(\Delta HA) + 0.0151(OPTT)(\Delta OA) + 0.0173(OPTT)^2. \quad (A2)$$

$$TT_{max} = 0.370 - 0.205(\alpha) + 0.0307(\Delta HA) + 0.108(\Delta OA) + 1.019(OPTT) - 0.135(\alpha)^2 + 0.0141(\Delta HA)(\alpha) + 0.0998(\Delta HA)^2 + 0.208(\Delta OA)(\alpha) - 0.0301(\Delta OA)(\Delta HA) - 0.226(\Delta OA)^2 + 0.353(OPTT)(\alpha) - 0.0497(OPTT)(\Delta OA) - 0.423(OPTT)^2 + 0.202(\Delta HA)(\alpha)^2 - 0.281(\Delta OA)(\alpha)^2 - 0.342(\Delta HA)^2(\alpha) - 0.245(\Delta HA)^2(\Delta OA) + 0.281(\Delta OA)^2(\Delta HA) - 0.184(OPTT)^2(\alpha) - 0.281(\Delta HA)(\alpha)(\Delta OA) \quad (A3)$$

$$X_{cc} = 0.153 - 0.322(\alpha) + 0.396(\Delta HA) + 0.424(\Delta OA) + 0.0226(OPTT) + 0.175(\alpha)^2 + 0.0185(\Delta HA)(\alpha) - 0.0701(\Delta HA)^2 - 0.251(\Delta OA)(\alpha) + 0.179(\Delta OA)(\Delta HA) + 0.0150(\Delta OA)^2 + 0.0134(OPTT)(\alpha) + 0.0296(OPTT)(\Delta HA) + 0.0752(OPTT)(\Delta OA) + 0.0192(OPTT)^2 \quad (A4)$$